Design and experimental characterization of a solar cooker with a prismatic cooking chamber and adjustable panel reflectors

# Design and experimental characterization of a solar cooker with a prismatic cooking chamber and adjustable panel reflectors

Alessia Aquilanti[a,b,*], Sebastiano Tomassetti[a], Matteo Muccioli[c], Giovanni Di Nicola[a]

[a] *Marche Polytechnic University, Department of Industrial Engineering and Mathematical Sciences, Via Brecce Bianche 12, 60131, Ancona (Italy)*
[b] *Technical University of Darmstadt, Institute of Construction and Building Materials, Franziska-Braun-Str. 3, 64287, Darmstadt (Germany)*
[c] *Studio MUMA, Via Eugenio Curiel 66 R, 47922, Rimini (Italy)*

**Abstract**

In this work, a novel solar cooker with the cooking chamber shaped like a Newton prism was designed, constructed and tested. The device is characterized by ease of construction, use and transportation. It is made of common and inexpensive materials. The proposed cooker is able to track the sun during its use through wheels placed at its base and a manual system to vary the inclination of the reflective surfaces. Experimental tests were carried out to characterize its thermal and optical performances and evaluate the wind's influence. In particular, two identical prototypes, one shielded from the wind and the other not, were simultaneously tested by tracking the reflective surfaces at optimal angles. Several tests were carried out without and with a load using water and glycerin as test fluids. The results showed that the solar cookers have good thermal performance even at medium-high temperatures. Both prototypes reached a stagnation temperature of about 137 °C. The shielded cooker usually brought 2 kg of water from 40 °C up to 90 °C in about two hours and 2 kg of glycerin from 40 °C up to 110 °C in less than three hours. These times were slightly longer for

*Corresponding author. Tel: +39 0712204277, fax: +39 0712204770
*Email addresses:* a.aquilanti@pm.univpm.it (Alessia Aquilanti), s.tomassetti@pm.univpm.it (Sebastiano Tomassetti), matteo.muccioli@gmail.com (Matteo Muccioli), g.dinicola@univpm.it (Giovanni Di Nicola)

the unshielded prototype.

*Keywords:* Solar cooking; Sun tracking; Experimental; Cooker opto-thermal ratio

## 1. Introduction

Currently, a significant percentage of the world's energy consumption is due to cooking purposes. This is especially true for various developing countries and rural areas of the world where, in some cases, more than 90% of the energy is consumed for cooking food [1]. However, in these areas, most of the energy demand for cooking is covered by non-commercial fuels, leading to harmful pollution and environmental problems [2, 3]. Since many developing countries are characterized by several days of the year with abundant solar radiation [4], solar cooking can be considered a sustainable alternative to the conventional energy sources used for cooking. Of course, this aspect is also valid for many developed countries. In fact, despite their shortcomings and limitations [5, 6], solar cookers are usually more affordable and less environmentally harmful than many of the most widespread cooking technologies.

In recent years, numerous designs of solar cookers characterized by different sizes and technologies have been reported in the literature [5, 7, 8, 9]. To overcome their limitations and improve their performances, various experimental and numerical studies analyzed possible modifications of solar cookers and their integration with thermal energy storage systems [6, 10, 11].

As explained by Aramesh et al. [5], solar cookers can be classified into three main structural types: panel cookers, box cookers and concentrating cookers. As they have the simplest design, the panel cookers are usually more cost-effective and easier to build than other types of solar cookers. Given their simplicity and flexibility, various designs of panel cookers have been developed in the last decades [5, 7, 12]. Some examples are the Cookit [13], the Solar Funnel Cooker [14], the Hot Pot [15], the Copenhagen Solar Cooker [16], and the Haines Solar Cookers [17].

Among the several designs of solar box cookers developed over the years, some very low-cost and simple prototypes have been designed and manufactured using inexpensive and recycled materials, such as cardboard boxes [12]. While various prototypes have been described in non-scientific literature (e.g., the Kyoto Solar Box Cooker [18] and the Jose Sol Cooker [19]), different scientific works presented designs and experimental characterizations of low-cost and simple box cookers. Some of the main literature studies concerning low-cost solar cookers are briefly described below.

Ozturk [20] manufactured a low-cost and simple solar box cooker from a plastic sheet box and a transparent plastic plate. The prototype was tested by using a commercial aluminum pot filled with water and its energy and exergy efficiencies were calculated. The results of the experimental tests showed that the average water temperature was only 73.2 °C, while the average energy and exergy efficiencies were 18.3 % and 2.2 %, respectively.

Mahavar et al. [21] designed a low-cost box cooker, known as Single Family Solar Cooker, that was tested with two aluminum cylindrical pots. The prototype has a small size and was manufactured using inexpensive materials. The experimental results showed that the cooker was able to cook two meals of soft load for two persons also in winter and its thermal performance parameters were comparable with those of other box solar cookers available in the literature.

Following the ASAE S580.1 Standard [22], Ebersviller and Jetter [23] experimentally compared the performances of a panel cooker, namely Hot Pot, with those of a parabolic cooker (Sun Chef Cooker) and a box cooker (Global Sun Oven). The prototypes were tested by using the load ratio recommended by the Standard, i.e., 7 kg of water per square meter of intercept area. A standardized cooking power for the panel cooker equal to 25 W was obtained, which is lower than the values obtained for the box cooker (65 W) and the parabolic cooker (198 W). This outcome could be due to the aperture area of the panel cooker lower than that of the other devices. The results obtained for other experimental parameters confirmed the lower performance of the Hot Pot.

Sagade et al. [24] experimentally analyzed the performance of a simple and

small solar box cooker with a booster reflector. A new parameter, namely effective concentration ratio, was defined to assess the effectiveness of the booster reflector. From the experimental tests performed with and without the booster reflector, it was found that the new parameter enabled the assessment of the effect of the booster reflector in the estimation of the opto-thermal performance of the studied device. Moreover, the authors experimentally investigated the thermal performance of the same solar box cooker tested with different working fluids [25] and a modified cooking pot [26].

The thermal performance of a simple solar box cooker with different reflector configurations were experimentally evaluated by Weldu et al. [27]. From the tests without load, the cooker with reflector tracking at the optimal angle provided the highest values of the stagnation temperature (145.4 °C) and the first figure of merit ($F_1 = 0.154$ °C/(W/m$^2$)). As expected, the results of the tests with water showed that the cooker configuration with reflector tracking at the optimal angle and an aluminum pot ensured better thermal performance than that of the configurations with a fixed angle of the reflector and a stainless steel pot.

Ruivo et al. [28] simultaneously tested two identical funnel cookers by following the ASAE S580.1 Standard [22] to investigate the influence of the type of pot lid. They used one cooking pot in each cooker surrounded by a transparent cover and covered with a glass lid and a black metal lid, respectively. A significant number of tests with water and a mixture of water and ice were performed in Malaga, Spain during a period with low sun elevation, with azimuthal solar tracking. The results showed that the pot with the glass lid gave a higher average standardized cooker power (73.9 W) than the pot with the black metal lid (50.6 W). Four configurations of the Copenhagen Solar Cooker were simultaneously tested by Apaolaza-Pagoaga et al. [29] under the same weather conditions. From the tests without load, it was found that the performance of one configuration is more influenced by the solar altitude angle than the others. The results of the tests with water carried out by partly following the ASAE S580.1 Standard [22] showed that the linear trend of the standardized power is

not universal, proving that the procedure for evaluating this parameter recommended by the Standard should be improved, as also demonstrated by Ruivo et al. [30, 31]. Recently, two prototypes of Haines 2 Solar Cooker were experimentally analyzed side-by-side by the same authors in Malaga, Spain [32]. The influence of the solar altitude angle on cooker performance was evaluated from the tests without load. Instead, the influence of the solar altitude angle and the impact of using partial loads on their thermal performance were analyzed from the tests with water. Based on their results, the authors suggested that the influence of both solar altitude angle and partial loads should be considered in future versions of ASAE S580.1 Standard [22].

In this study, a low-cost and simple solar cooker having an innovative variable geometry, named Newton solar cooker (NSC), is presented. The proposed solar cooker was experimentally tested and its performance expressed in terms of efficiency was investigated. In particular, the purpose of this study was to simultaneously test two identical NSC prototypes, one wind-shielded and the other not, to determine their performances, also considering the influence of wind. The following experimental outdoor campaign was developed: 3 tests without load, 4 water tests and 4 glycerin tests were carried out. The methodology followed to perform the tests is the same proposed in some of our previous works [33, 34] and allows us to evaluate the main performance parameters used in the scientific literature.

The paper is divided into the following sections. In Section 2, the characteristics of the NSC and the optical analysis of the device are discussed. The optimal inclination angles of the primary and secondary reflectors for different elevations of the sun obtained by a 2D model are also reported. Section 3 describes the manufacturing steps of the prototype along with the materials used. A cost analysis of all components is also given in this section. Section 4 defines the experimental parameters used to characterize the two tested devices and the experimental setup designed for the outdoor campaign. Section 5 reports the results of the study, dividing them between no-load, water-loaded and glycerin-loaded tests. The conclusions of the article are given in Section 6.

## 2. Design and optical analysis

The new solar cooker presented in this work, shown in Fig. 1, is based on designs of a solar cooker with the cooking chamber shaped like a Newton prism, named Newton solar cooker (NSC) [35, 36], developed by Matteo Muccioli, co-author of this work. In general, the NSC was designed to be easy to build and use; in fact, its main strengths are the ease of construction, the ease of movement and transportation, and the use of common and inexpensive materials. The device can be constructed quickly since only common tools are required. It can be easily transported since it can be easily disassembled and resealed. Moreover, the presented solar cooker is affordable and easy to replicate because it can be made of readily available materials with a quasi-zero cost.

Starting from the original versions of the NSC, which were never investigated in scientific works, the construction features of the new version were chosen to improve its thermal and optical performances. In this regard, the modifications performed on the proposed NSC were based on some preliminary outdoor tests where different insulating and reflecting materials and geometrical configurations were evaluated. Fig. 2 shows the working scheme of the new device presented here. It consists of a glass prism cooking chamber made of two tempered glass panes, a wooden panel placed at the base and two side doors. The glass panes are supported by the two side panels and the two side doors. A layer of thermal insulating material and a steel plate are placed at the base of the chamber. Moreover, the device comprises two rotating reflector support structures placed at the sides of the chamber: a longer support for the primary reflective surface and a shorter one for the secondary reflective surface. A detailed description of the construction of the presented prototype is reported in Section 3.

From Fig. 2, it can be understood that the device's geometry can be changed by varying $\theta_1$ and $\theta_2$, i.e., the inclination angles of the primary and secondary reflectors with respect to the horizontal plane, respectively. This results in a change in the NSC aperture area ($A_\mathrm{a}$). The area $A_\mathrm{a}$ is calculated as the

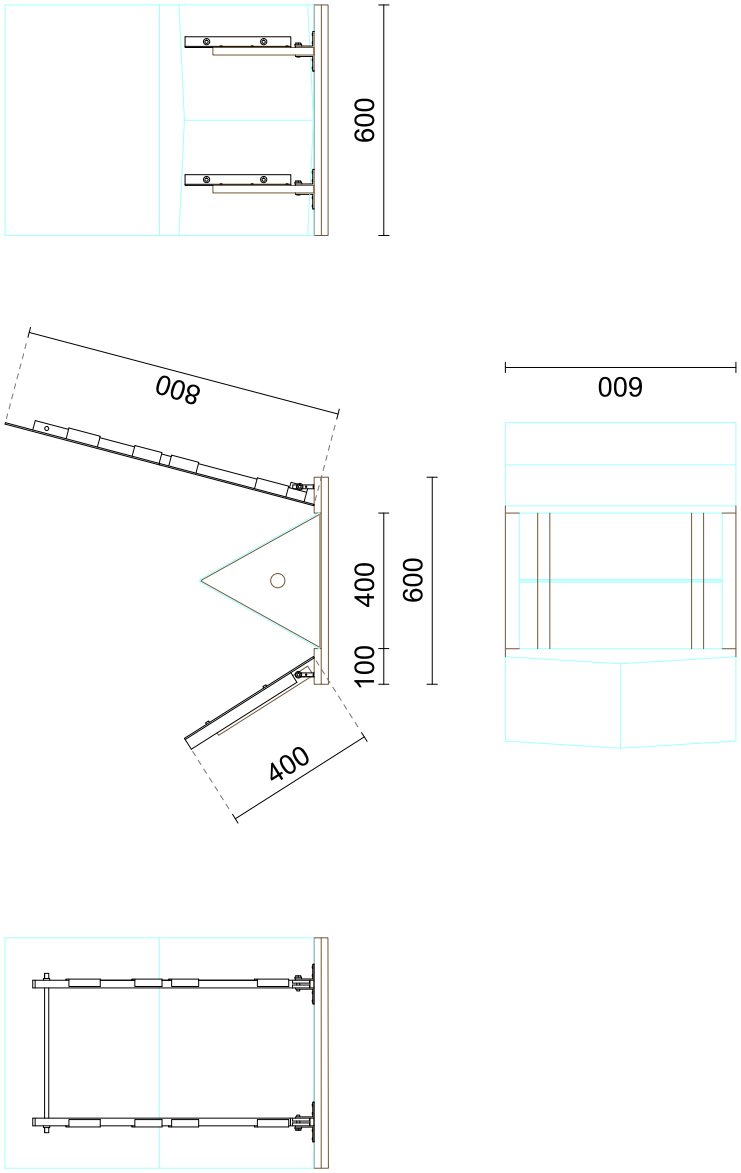


Fig. 1: Newton solar cooker views (dimensions in mm).

projection of the area bounded by the outer edges of the prototype on a plane perpendicular to the direction of the sun's rays. By optimizing the values of $\theta_1$ and $\theta_2$ according to the elevation of the sun ($H_{\text{sun}}$), it is possible to maximize the amount of solar radiation concentrated on the steel plate where the pot is placed.

To calculate optimal $\theta_1$ and $\theta_2$ values associated with different sun elevations, a simplified 2D model to simulate the propagation of the solar rays on the surfaces of the solar cooker was developed using MATLAB software [37]. In the model, the solar rays are represented by vectors with an initial unit modulus from the sun's direction. The solar cooker surfaces are modeled as obstacles to the propagation of sun rays, dividing them between reflective surfaces (the two reflectors) and glazed surfaces (the two glasses), according to the prototype design. In particular, the reflective surfaces are characterized by specific values of $\theta_1$ and $\theta_2$. During the simulation, the sun's rays impact the various surfaces of the solar cooker, which cause either reflection, transmission or absorption. To compute the final amount of concentrated energy more realistically, the transmittance and reflectance values of the materials are used to correct the modulus of the solar ray vectors at each transmission or reflection. The model also takes into account possible multiple reflections between reflectors. A ray is no longer propagated in the following two cases: the ray does not impact the cooker or the ray hits the cooker surface where the pot is placed. The rays' moduli that meet the first condition are neglected, while those that meet the second condition are summed. The score assigned to a specific configuration of $\theta_1$ and $\theta_2$ for a given $H_{\text{sun}}$ is the sum of rays' moduli obtained at the end of the simulation of the rays' propagation.

For the latitude of Ancona, Italy (latitude of 43.5871°N), discretized with 1-degree steps, the optimal configurations of $\theta_1$ and $\theta_2$ values that got the highest scores were determined using the Particle Swarm Optimization algorithm [38]. As an example, the optimal values of $\theta_1$ and $\theta_2$ at 12:00 solar time on the days of the equinox, summer solstice and winter solstice are reported below:

- Spring Equinox, 20/03/2022: $H_{\text{sun}} = 46.24°$, $\theta_1 = 76.40°$, $\theta_2 = 22.99°$;
- Summer Solstice, 21/06/2022: $H_{\text{sun}} = 69.79°$, $\theta_1 = 96.09°$, $\theta_2 = 47.62°$;
- Winter Solstice, 21/12/2022: $H_{\text{sun}} = 22.97°$, $\theta_1 = 56.49°$, $\theta_2 = 2.33°$.

Fig. 3 shows the score (on the z-axis) for each pair of $\theta_1$ (x-axis) and $\theta_2$ (y-axis), again for 12:00 solar time on the equinox, summer solstice, and winter solstice days.

To adjust the solar cooker geometry according to the sun elevation, the optimal $\theta_1$ and $\theta_2$ pairs associated with each sun elevation were used by the operator during the experimental campaign. Table 1 shows the optimal values of $\theta_1$ and $\theta_2$ for $H_{\text{sun}}$ between 50 and 70°, with the corresponding aperture area of the NSC.

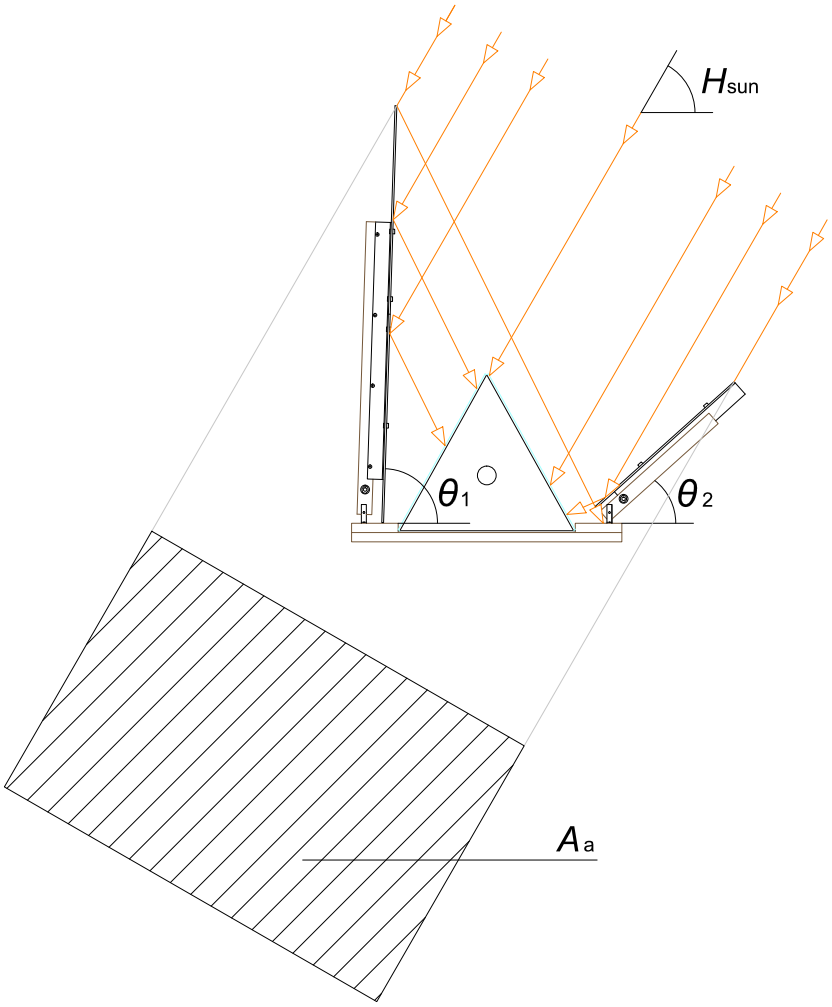


Fig. 2: Working scheme of the Newton solar cooker.

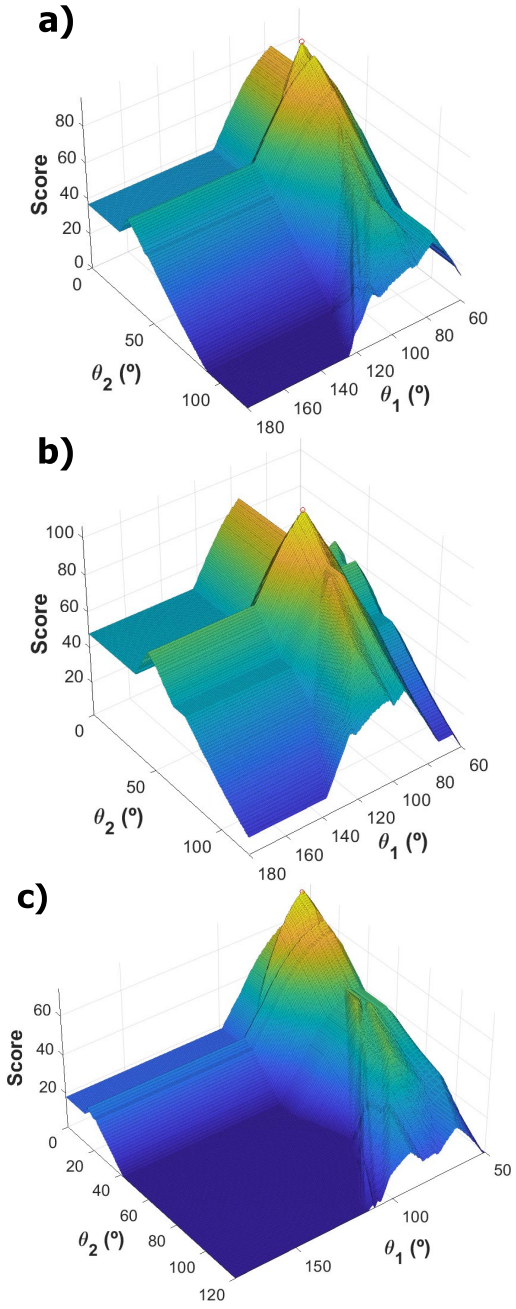


Fig. 3: Score (z-axis) obtained by a 2D model for the distribution of the solar radiation on the NSC for each pair of $\theta_1$ (x-axis) and $\theta_2$ (y-axis) at 12:00 solar time: a) Spring Equinox, 20/03/2022; b) Summer Solstice, 21/06/2022; c) Winter Solstice, 21/12/2022.

Table 1: Newton solar cooker optimal configurations in Ancona for different sun elevations and corresponding aperture areas.

| $H_{\text{sun}}$ (°) | $\theta_1$ (°) | $\theta_2$ (°) | $A_{\text{a}}$ ($\text{m}^2$) |
|---|---|---|---|
| 50 | 80.29 | 34.72 | 0.394 |
| 52 | 81.21 | 35.92 | 0.396 |
| 54 | 83.16 | 37.44 | 0.401 |
| 56 | 84.28 | 39.48 | 0.401 |
| 58 | 86.43 | 39.93 | 0.410 |
| 60 | 88.10 | 41.79 | 0.413 |
| 62 | 90.28 | 42.67 | 0.421 |
| 64 | 91.19 | 43.82 | 0.421 |
| 66 | 93.18 | 44.99 | 0.426 |
| 68 | 94.06 | 46.83 | 0.423 |
| 70 | 96.85 | 47.76 | 0.434 |

## 3. Manufacture and assembly

The manufacturing steps of the proposed Newton solar cooker, shown in Fig. 1, are the following: 1) construction of the base panel; 2) cutting and assembly of supports; 3) construction of the side doors; 4) construction of the cooking chamber; 5) arrangement of the reflectors and final assembly. Each step is described in this section. In addition, details about manufacturing costs are provided.

### *3.1. Construction of the base panel*

A $600 \times 600 \times 20$ mm multilayer poplar wood panel was used as the base on which the other elements of the cooker rest. Two poplar wood panels measuring $600 \times 100 \times 20$ mm were fixed with screws at the top of the base panel along two opposite edges. Their task is to keep two tempered glass panes that form the glass prism cooking chamber in position, preventing them from sliding outwards and guaranteeing the closure of the cooking chamber. To facilitate the prototype's usage and ensure its manual alignment to solar radiation, the base panel was fitted with 3 wheels.

### *3.2. Cutting and assembly of supports*

To form the support arms for the primary panel reflectors, two bars with a length of 650 mm were cut using a metal saw starting from a square steel hollow profile with a $20 \times 20$ mm cross-section. As shown in Fig. 4a, the square metal bars were fixed and anchored to the base of the solar cooker using angle brackets. The angle brackets were fastened to the bars using a self-locking system to allow the entire support system to change the angle for proper sun tracking. The primary reflectors were fastened to the support arms through eight 100-mm-long pieces that were first cut from an aluminum C-profile and then attached vertically to the reflectors using double-sided adhesive tape. In addition, the two square bars were fixed together with a metal rod at the top to make the entire system more stable.

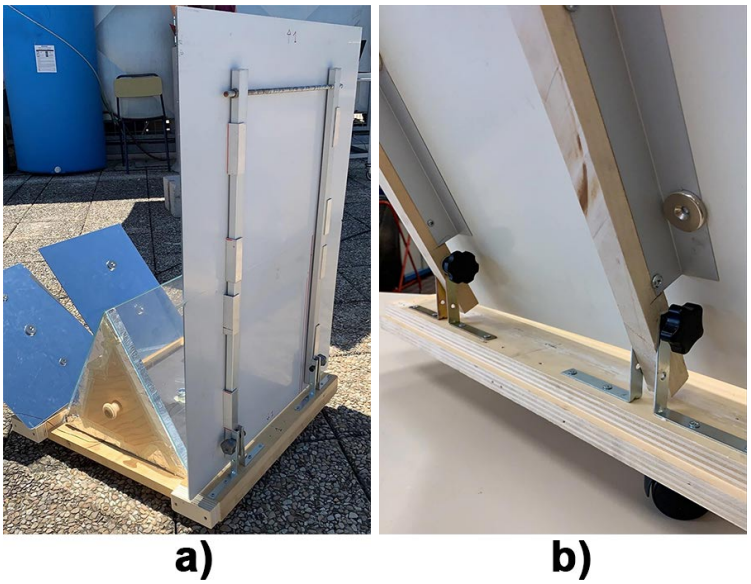


Fig. 4: Detail of the connection of the reflector supports to the wooden base: a) primary reflectors and b) secondary reflectors.

To form the support arms for the secondary reflectors, two profiles of 300 mm in length were cut using an aluminum saw starting from a 1000 mm long aluminum L-profile with a $30 \times 30$ mm cross-section. To make the reflector supports more stable during use, the aluminum profiles were reinforced by joining them to 350 mm long wooden strips with a $20 \times 20$ mm square section. As evident in Fig. 4b, the wooden supports were fixed and anchored to the base of the solar cooker in the same way as the square metal bars. The secondary reflectors were fixed to the aluminum supports and held in position by magnets.

### *3.3. Construction of the side doors*

In addition to the base panel and glass surfaces, the cooking chamber was obtained by using two side doors that support the glass surfaces. The side doors, made of solid fir wood, are in the shape of an isosceles triangle with dimensions $400 \times 332 \times 30$ mm and are fitted with a handle on one side to facilitate their movement during testing. Moreover, the mobile doors allow varying the volume of the cooking chamber, adapting it to the pot and the load being used.

An aluminum film was applied to the handle-free surface of the triangular doors and secured with adhesive tape with a twofold purpose: to reflect the direct sun's rays at the doors inside the cooking chamber, thus reducing the dispersion of radiation, and to prevent that the steam generated inside the cooking chamber penetrates the wood of the doors, affecting its thermal insulation resistance.

### *3.4. Construction of the cooking chamber*

The base of the cooking chamber was thermally insulated by inserting a $430 \times 375 \times 8$ mm cork panel over the poplar wood base. The cork panel was shaped to fit perfectly into the section created between the poplar base and the two side panels anchored to it. A steel plate measuring $420 \times 365 \times 1$ mm was placed on top of the cork layer. The plate was painted with a high-performance black paint to increase its ability to absorb heat from solar radiation.

Two panes of tempered extra-clear glass measuring $380 \times 480$ mm and 4 mm thick make up the actual cooking chamber. The two panes of glass were placed on the triangular side doors and held in place by the two poplar wood panels. A gap was left on the top to prevent condensation inside the cooking chamber by spacing the two glass panes about 2 mm. This allows for improving the cooking performance of the device.

### *3.5. Arrangement of the reflectors and final assembly*

Polymethylmethacrylate (PMMA) sheets were used for the reflective surfaces because of the material's low cost and to allow the operator to work safely. The presented configuration consists of 4 reflectors on 3 planes. The primary reflective surface consists of two $600 \times 400$ mm reflectors placed one above the other on the same plane, thus forming a single $600 \times 800$ reflector. The secondary reflective surface is made up of two $300 \times 400$ mm reflectors in a V configuration. The four reflectors were fixed to the supports, as described in Section 3.2.

### *3.6. Cost analysis*

Table 2 shows the materials used for the construction of the prototype, with the related costs. The highest costs are given by the PMMA reflectors, the extra-clear tempered glass and the steel plate. These are the components that most influence the optical (the first two) and thermal efficiency (the last one) of the device. It is evident that the use of recycled or widely used materials, such as wood, to make the main parts of the device (i.e., the base structure, the side doors and the reflector supports) helped to keep the final cost low. The prototype construction took two working days by a team of two unskilled workers.

Table 2: Cost analysis of the prototype.

| Item | Cost (EUR) |
|---|---|
| Panel reflectors | 45.00 |
| Extra clear tempered glass | 40.00 |
| Steel plate | 30.00 |
| Wood (structural frame, side doors and handles) | 15.00 |
| Aluminum L-profile | 10.00 |
| Insulating cork layer | 10.00 |
| Miscellaneous | 40.00 |
| Total | 190.00 |

## 4. Experimental tests and setup

In this section, the types of tests carried out, the test fluids chosen and the instrumentation used in the outdoor experimental campaign are described. Then, the main parameters used to characterize the NSC are presented.

### *4.1. Experimental setup*

Fig. 5 shows the experimental setup used during the experimental campaign. Two identical prototypes of NSC were placed on the ground and tested simultaneously under the same outdoor conditions. One of the two devices was shielded with a wind shielding system specifically constructed for the experimental campaign. The cooking chamber of each prototype was loaded with a black stainless-steel pot containing the fluid to be tested. The pot has a diameter of 200 mm, a height of 130 mm, a thickness of 2 mm and a mass of 476 g.

The recorded quantities during the tests were the absorber plate temperatures of the two devices ($T_{\mathrm{a}}$), the fluid temperatures inside the pots ($T_{\mathrm{f}}$), the ambient temperature ($T_{\mathrm{amb}}$), the direct normal solar irradiance ($G_{\mathrm{bn}}$), and the global horizontal solar irradiance ($G$).

The sensors used to record the temperatures were T-type thermocouples with an uncertainty of $\pm 1\,^{\circ}\mathrm{C}$. In detail, the one used to record the fluid temperature was immersed in the studied fluid and held in place throughout the test. The thermocouple for the absorber plate temperature was fixed to the plate using high-temperature adhesive tape, shielding it from direct exposure to the sun. Instead, the one used to record the ambient temperature was placed in a shady place to avoid influencing the measurement.

The direct normal solar irradiance was recorded using an Eppley NIP pyrheliometer (normal incidence pyrheliometer) with a one-second response and linearity $\pm 0.5\%$ from 0 to $1400\,\mathrm{W/m^2}$. T-thermocouples and pyrheliometer signals were collected by a Pico Technology TC-08 datalogger and sent to a computer. The global horizontal solar irradiance was measured using a pyranometer SR30-M2-D1 with linearity $\pm 3.0\%$ from 0 to $4000\,\mathrm{W/m^2}$ placed horizontally near the

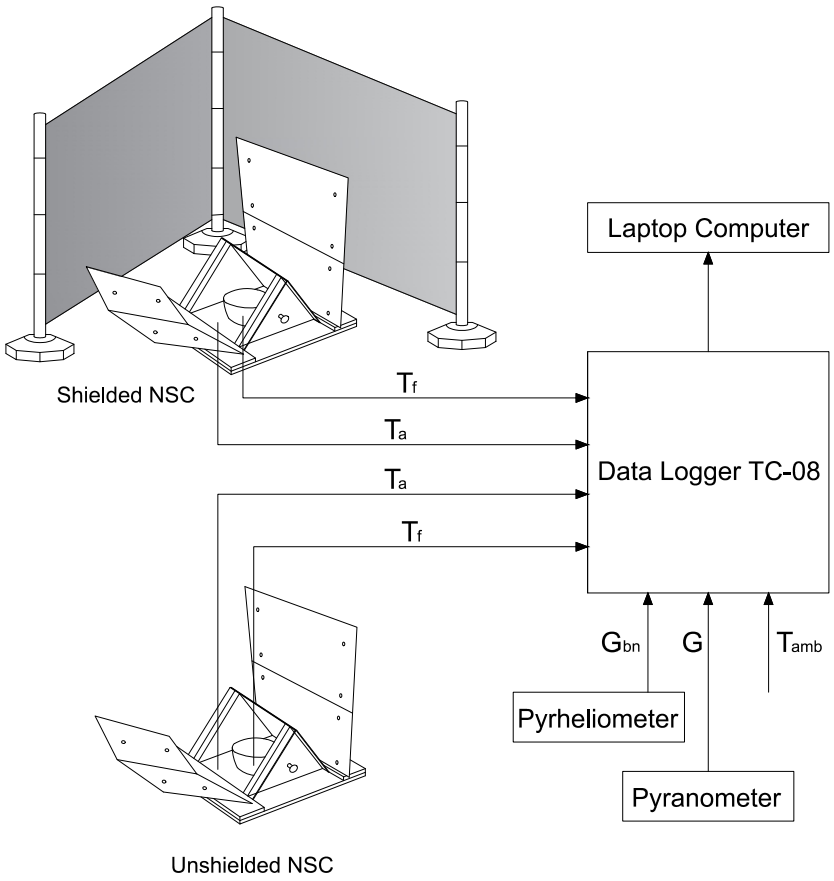


Fig. 5: Experimental setup. $T_{\mathrm{a}}$: absorber temperature; $T_{\mathrm{f}}$: testing fluid temperature; $T_{\mathrm{amb}}$: ambient temperature; $G_{\mathrm{bn}}$: direct normal solar irradiance; $G$: global horizontal solar irradiance.

tested prototypes. By following the same procedure described by other authors [28, 29, 32, 39], the global normal solar irradiance ($G_{\mathrm{n}}$) was calculated using the Liu Jordan isotropic sky model [40] considering an albedo of 0.2.

### *4.2. Experimental parameters*

Given the growing interest in the study and manufacture of solar cookers, there is a need for common procedures and standards to be followed for the characterization of the prototypes under investigation. These standards indicate the parameters and procedures to be followed to characterize the optical and

thermal performance of these devices.

Table 3 shows the parameters used to characterize the NSC performance during the tests with and without load. The experimental campaign was divided into two phases: the first tests were carried out by testing the devices without load while all the remaining tests were carried out by loading the cooking chamber with a fluid. The first tests with no load were used to reach the stagnation condition of the devices, i.e., the balance between heat input and heat loss output. These tests are necessary to identify the first figure of merit ($F_1$) associated with the device. It should be noted that for the determination of $F_1$ (Table 3), the considered values of ambient temperature ($T_{\mathrm{amb}}$) and global normal solar irradiance ($G_{\mathrm{n}}$) are those associated with the maximum temperature value reached by the plate during the test.

Load tests were carried out by loading the cooking chamber of each device with a black painted pot containing a test fluid. The selected fluids were water and glycerin. Water was selected because the obtained results could be easily comparable with those obtained by other researchers. Glycerin was selected because it is widely used to test the performance of solar cookers [25, 26, 39].

For the tests with water, as suggested by Funk [45], the parameters described in Table 3 were calculated over a time interval $\Delta t_{\mathrm{h}}$ required to raise the temperature of the fluid from 40 °C to 90 °C. In addition, the parameters were adapted and calculated to determine the behavior of the devices under investigation when tested with glycerin. The selected glycerin temperature range within which all parameters were calculated was 40–110 °C.

Lahkar et al. [44] proposed a procedure to determine the cooker opto-thermal ratio (COR) starting from the Hottel-Whillier-Bliss equation for solar cookers:

$$\eta = F'\eta_0 - \left(\frac{F'U_{\mathrm{l}}}{C}\right)\chi, \tag{1}$$

where $\chi = (T_{\mathrm{f}} - T_{\mathrm{amb}})/G_{\mathrm{n}}$. The parameters $F'\eta_0$ and $F'U_{\mathrm{l}}/C$ of the equation can be identified from the data obtained from the experimental tests. These are

Table 3: Experimental parameters for the characterization of the Newton solar cooker.

| Experimental parameter | Equation | Equation parameters |
|---|---|---|
| First figure of merit [41] | $F_1 = \frac{T_{\mathrm{a,max}} - T_{\mathrm{amb}}}{G_{\mathrm{n}}}$ | $A_{\mathrm{a}}$ = aperture area of the solar cooker |
| | | $c_{\mathrm{f}}$ = specific heat of the test fluid |
| Heating time interval | $\Delta t_{\mathrm{h}} = t(T_2) - t(T_1)$ | $C$ = geometrical concentration ratio |
| | | $G_{\mathrm{n}}$ = global normal solar irradiance |
| Second figure of merit [41] | $F_2 = \frac{F_1 m_{\mathrm{f}}\, c_{\mathrm{f}}}{A_{\mathrm{a}} \Delta t_{\mathrm{h}}} \ln \left[ \frac{1 - \frac{1}{F_1}(T_1 - T_{\mathrm{amb,av}})/G_{\mathrm{n,av}}}{1 - \frac{1}{F_1}(T_2 - T_{\mathrm{amb,av}})/G_{\mathrm{n,av}}} \right]$ | $G_{\mathrm{n,av}}$ = mean $G_{\mathrm{n}}$ measured at $\Delta t_{\mathrm{h}}$ |
| | | $G_{\mathrm{n,ref}} = 900\,\mathrm{W/m^2}$ (for $t_{\mathrm{s}}$ calculation) |
| Specific boiling time [42] | $t_{\mathrm{s}} = \frac{\Delta t_{\mathrm{h}} A_{\mathrm{a}}}{m_{\mathrm{f}}}$ | $\eta_0$ = optical efficiency |
| | | $F'$ = heat exchange efficiency factor |
| Characteristic boiling time [42] | $t_{\mathrm{ch}} = t_{\mathrm{s}} \frac{G_{\mathrm{n,av}}}{G_{\mathrm{n,ref}}}$ | $m_{\mathrm{f}}$ = mass of the test fluid |
| | | $T_{\mathrm{amb}}$ = ambient temperature |
| Overall efficiency [42] | $\eta_{\mathrm{av}} = \frac{m_{\mathrm{f}}\, c_{\mathrm{f}} (T_2 - T_1)}{G_{\mathrm{n,av}} A_{\mathrm{a}} \Delta t_{\mathrm{h}}}$ | $T_{\mathrm{a,max}}$ = absorber stagnation temperature |
| | | $T_{\mathrm{amb,av}}$ = mean $T_{\mathrm{amb}}$ measured at $\Delta t_{\mathrm{h}}$ |
| Utilizable efficiency [43] | $\eta_{\mathrm{u}} = \frac{m_{\mathrm{f}}\, c_{\mathrm{f}} (T_2 - T_{\mathrm{amb,av}})}{G_{\mathrm{n,av}} A_{\mathrm{a}} \Delta t_{\mathrm{h}}}$ | $T_{\mathrm{f,av}}$ = mean $T_{\mathrm{f}}$ measured at $\Delta t_{\mathrm{h}}$ |
| | | $t(T_1)$ = starting time of the heating phase |
| Cooker opto-thermal ratio [44] | $COR = \frac{\eta_0 C}{U_{\mathrm{l}}}$ | $t(T_2)$ = ending time of the heating phase |
| | | $U_{\mathrm{l}}$ = heat loss factor |
| Maximum achievable fluid temperature [44] | $T_{\mathrm{fx}} = T_{\mathrm{amb,av}} + \frac{F' \eta_0 G_{\mathrm{n,av}}}{F' U_{\mathrm{l}} / C}$ | |

the intercept and the opposite value of the slope of the efficiency line regression.

The total time interval to cover the chosen temperature range for water (40–90 °C) and glycerin (40–110 °C) is divided into sub-intervals of 5 minutes each. For each sub-interval, the average global normal solar irradiance, the average ambient temperature, the average test fluid temperature, the efficiency and the parameter $\chi$ are determined. Plotting the thermal efficiency $\eta$ against the parameter $\chi$ for each identified sub-interval, it is possible to identify the regression line of the efficiency curve and its coefficient of determination $R^2$. The regression line's intercept and opposite value of the slope correspond to the parameters $F'\eta_0$ and $F'U_1/C$, which are necessary for the determination of the $COR$ parameter.

Finally, it is worth to point out that the ASAE S580.1 Standard [22] procedure for the calculation of the standardized power was not used here because it is not physically consistent, as recently showed by Ruivo et al. [46].

### *4.3. Experimental tests*

The experimental campaign was carried out in June 2021 on the roof of the Department of Industrial Engineering and Mathematical Sciences (latitude 43.5871°N, longitude 13.5149°E). As mentioned above, two identical Newton solar cooker prototypes were made and tested at the same time avoiding shaded areas in the test area. To understand the wind effect, one of the two devices was shielded from the wind during the tests.

With reference to wind intensity, Fig. 6 shows the average wind speed recorded in a location near the testing area (latitude 43.6098°N, longitude 13.5105°E) during the time slot when the measures were conducted. The data were collected from the website of the Marche Region – Civil Protection Service [47]. It is evident that, in all the tests, these values exceed the limit of 1 m/s imposed by the ASAE standard [22, 48]. For this reason, following the same strategy adopted by other authors [23], the prototypes were tested by placing them near the parapets and walls of buildings, shielding them from direct wind exposure.

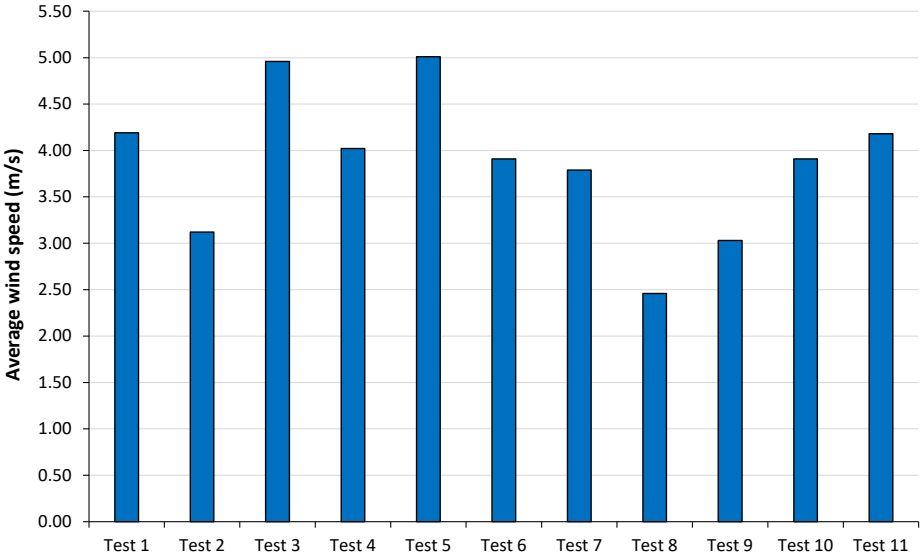


Fig. 6: Average wind speed recorded in Ancona, Italy during the testing period.

During the tests, the operator maintained the cooking chamber and the reflector system of the two devices always pointed towards the sun direction. Additionally, to make the best use of the reflective surfaces and to concentrate as much solar radiation as possible into the cooking chamber, the elevation of the sun ($H_{\text{sun}}$) was checked every 20 minutes and the $\theta_1$ and $\theta_2$ angles of the primary and secondary reflective surfaces were adjusted according to Table 1. Every tested configuration of the cooker was recorded by the operator in terms of $H_{\text{sun}}$, $\theta_1$ and $\theta_2$ angles. These values were averaged across the test duration to obtain $H_{\text{sun,av}}$, $\theta_{1,\text{av}}$ and $\theta_{2,\text{av}}$ for each test. The average aperture area ($A_{\text{a,av}}$) was calculated in a similar fashion. These quantities were used for the calculation of the parameters.

## 5. Experimental results

In this section, the results obtained from tests conducted with and without load are reported.

Table 4: Summary of tests without load.

| Quantity | Test 1 | | Test 2 | | Test 3 | |
|---|---|---|---|---|---|---|
| Date | 31/05/2021 | | 03/06/2021 | | 30/06/2021 | |
| Type of cooker | Unshielded | Shielded | Unshielded | Shielded | Unshielded | Shielded |
| $H_{\mathrm{sun,av}}$ (°) | 65.64 | 65.64 | 56.22 | 56.22 | 62.34 | 62.34 |
| $\theta_{1,\mathrm{av}}$ (°) | 92.48 | 92.48 | 84.90 | 84.90 | 89.98 | 89.98 |
| $\theta_{2,\mathrm{av}}$ (°) | 45.14 | 45.14 | 38.83 | 38.83 | 42.93 | 42.93 |
| $A_{\mathrm{a,av}}$ ($\mathrm{m}^2$) | 0.425 | 0.425 | 0.401 | 0.401 | 0.421 | 0.421 |
| $T_{\mathrm{amb}}$ (°C) | 21.07 | 20.99 | 30.05 | 29.70 | 32.60 | 33.40 |
| $G_{\mathrm{n}}$ ($\mathrm{W/m^2}$) | 981.19 | 977.35 | 908.86 | 907.25 | 936.19 | 932.46 |
| $G_{\mathrm{bn}}$ ($\mathrm{W/m^2}$) | 925.74 | 923.02 | 866.71 | 865.17 | 859.29 | 858.67 |
| $T_{\mathrm{a,max}}$ (°C) | 125.66 | 120.81 | 137.47 | 137.36 | 133.95 | 129.07 |
| $F_1$ (°C/($\mathrm{W/m^2}$)) | 0.107 | 0.102 | 0.118 | 0.119 | 0.108 | 0.103 |

### *5.1. Tests without load*

Three tests without load were carried out under different external conditions. Table 4 shows the environmental conditions associated with the maximum temperature reached by the absorber plate ($T_{\mathrm{a,max}}$) and the $F_1$ parameter calculated for each device in each test. Table 4 also shows the average sun elevation ($H_{\mathrm{sun,av}}$), the average angles $\theta_1$ and $\theta_2$ and the average aperture area ($A_{\mathrm{a,av}}$) for the reported tests. From Table 4, it can be noted that similar values of $T_{\mathrm{a,max}}$ and $F_1$ were obtained for the two devices in each test. The temperature trends of the absorber plate of the unshielded and shielded NSC prototypes for the test of 03/06/2021 (test 2) are shown in Fig. 7. As can be seen, the maximum temperature reached by the absorber plate was about 137 °C for both NSC prototypes. This maximum temperature ($T_{\mathrm{a,max}}$) was associated with a global normal solar irradiance and an ambient temperature of 908.86 $\mathrm{W/m^2}$ and 30.05 °C for the unshielded NSC and 907.25 $\mathrm{W/m^2}$ and 29.70 °C for the shielded NSC.

For the three tests without load, the following average values of the $F_1$ were obtained: $F_{1,\mathrm{av}} = 0.111\,^{\circ}\mathrm{C/(W/m^2)}$ for the unshielded device and $F_{1,\mathrm{av}} = 0.108\,^{\circ}\mathrm{C/(W/m^2)}$ for the shielded prototype. The values of $F_{1,\mathrm{av}}$ were used for

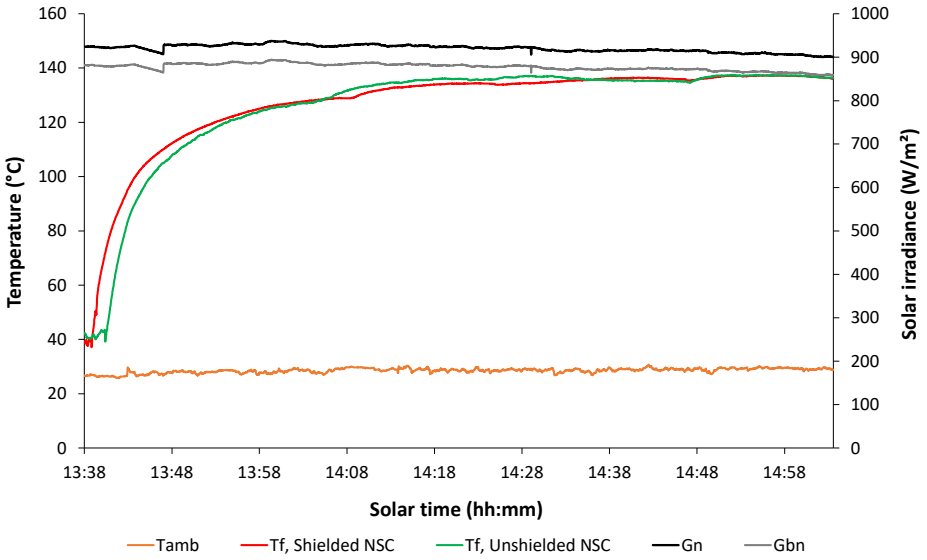


Fig. 7: Test without load (03/06/2021, test 2).

calculating the second figure of merit ($F_2$) for the tests with the load.

### *5.2. Tests with water*

Four outdoor tests were performed by loading each NSC device with 2 kg of water. Table 5 shows the main parameters for each test calculated in the fluid temperature range between 40 and 90 °C.

Fig. 8 shows the trends of water temperatures, ambient temperature and global and direct normal solar irradiances for test 4 (01/06/2021). The average global normal solar irradiance was 1050.80 W/m$^2$, while the average ambient temperature was 21.65 °C. The fluid took 127 minutes when tested with the unshielded NSC and 128 minutes when tested with the shielded device to go from 40 °C to 90 °C.

Fig. 9 shows the water trends obtained with the two prototypes during all water tests. From Fig. 9, it is possible to see that, even though the tests were carried out on days characterized by different solar irradiances and ambient temperatures, the trends in water temperatures are very similar. It can also be noted that, in each test, the time taken for the water to reach 90 °C was

Table 5: Summary of tests with water.

| | Test 4 | | Test 5 | | Test 6 | | Test 7 | |
|---|---|---|---|---|---|---|---|---|
| Date | 01/06/2021 | | 01/06/2021 | | 09/06/2021 | | 17/06/2021 | |
| Type of cooker | Unshielded | Shielded | Unshielded | Shielded | Unshielded | Shielded | Unshielded | Shielded |
| $H_{\mathrm{sun,av}}$ (°) | 58.60 | 58.60 | 61.26 | 61.26 | 63.13 | 63.13 | 62.96 | 62.96 |
| $\theta_{1,\mathrm{av}}$ (°) | 87.04 | 87.04 | 88.81 | 88.81 | 90.46 | 90.46 | 90.41 | 90.41 |
| $\theta_{2,\mathrm{av}}$ (°) | 39.59 | 39.59 | 41.98 | 41.98 | 43.45 | 43.45 | 43.26 | 43.26 |
| $A_{\mathrm{a,av}}$ ($\mathrm{m}^2$) | 0.411 | 0.411 | 0.416 | 0.416 | 0.417 | 0.417 | 0.419 | 0.419 |
| $m_{\mathrm{f}}$ (kg) | 2.0 | 2.0 | 2.0 | 2.0 | 2.0 | 2.0 | 2.0 | 2.0 |
| $T_1$ (°C) | 40 | 40 | 40 | 40 | 40 | 40 | 40 | 40 |
| $T_2$ (°C) | 90 | 90 | 90 | 90 | 90 | 90 | 90 | 90 |
| $G_{\mathrm{n,av}}$ ($\mathrm{W/m}^2$) | 1051.95 | 1049.64 | 951.90 | 954.14 | 824.15 | 830.93 | 918.31 | 918.31 |
| $G_{\mathrm{bn,av}}$ ($\mathrm{W/m}^2$) | 908.40 | 906.41 | 908.93 | 911.07 | 696.92 | 702.65 | 738.05 | 738.12 |
| $T_{\mathrm{amb,av}}$ (°C) | 22.03 | 21.99 | 23.69 | 23.59 | 23.76 | 23.54 | 30.22 | 30.21 |
| $\Delta t_{\mathrm{h}}$ (min) | 127 | 128 | 122 | 118 | 170 | 134 | 112 | 113 |
| $t_{\mathrm{s}}$ ($\mathrm{h\,m}^2/\mathrm{kg}$) | 0.44 | 0.44 | 0.42 | 0.41 | 0.59 | 0.47 | 0.39 | 0.40 |
| $t_{\mathrm{ch}}$ ($\mathrm{h\,m}^2/\mathrm{kg}$) | 0.51 | 0.51 | 0.45 | 0.43 | 0.54 | 0.43 | 0.40 | 0.40 |
| $\eta_{\mathrm{av}}$ | 0.13 | 0.13 | 0.15 | 0.15 | 0.12 | 0.15 | 0.16 | 0.16 |
| $\eta_{\mathrm{u}}$ | 0.17 | 0.17 | 0.19 | 0.20 | 0.16 | 0.20 | 0.19 | 0.19 |
| $F_2$ | 0.21 | 0.21 | 0.25 | 0.27 | 0.24 | 0.31 | 0.26 | 0.26 |
| $F'\eta_0$ | 0.247 | 0.255 | 0.271 | 0.329 | 0.285 | 0.345 | 0.279 | 0.268 |
| $F'U_{\mathrm{l}}/C$ ($\mathrm{W/m}^2\,°\mathrm{C}$) | 2.722 | 2.866 | 2.683 | 3.750 | 2.879 | 3.424 | 2.804 | 2.552 |
| $COR$ ($\mathrm{W/m}^2\,°\mathrm{C}$) | 0.091 | 0.089 | 0.101 | 0.088 | 0.099 | 0.101 | 0.100 | 0.105 |
| $T_{\mathrm{fx}}$ (°C) | 117.56 | 115.37 | 119.93 | 107.24 | 105.19 | 107.26 | 121.68 | 126.49 |
| $R^2$ | 0.974 | 0.941 | 0.867 | 0.886 | 0.910 | 0.909 | 0.929 | 0.948 |

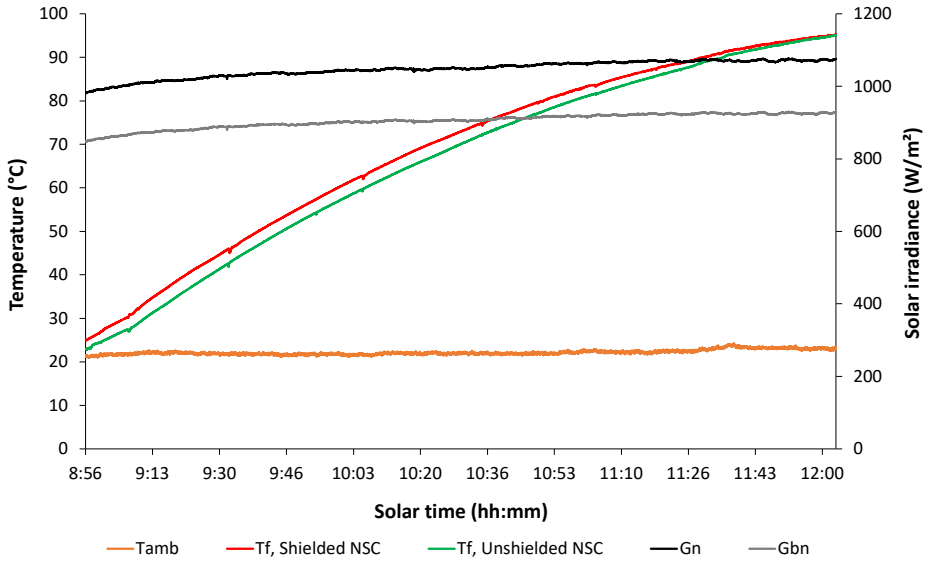


Fig. 8: Test with water (01/06/2021, test 4).

about the same for the two devices. In detail, this time was slightly longer in the case of the unshielded device (on average 133 minutes) with respect to the shielded one (on average 123 minutes). A decrease in the time required by the fluid tested in the shielded prototype is evident in test 6 (09/06/2021). The time taken by the unshielded NSC was 170 minutes while the time taken by the shielded device was 134 minutes.

In general, the shortest time was recorded in the test of 17/06/2021 (test 7): 112 minutes for the unshielded NSC and 113 minutes for the shielded NSC. During the test an average global normal solar irradiance of 918.31 $\mathrm{W/m^2}$ and an average ambient temperature of 30.22 °C were recorded. Comparing tests 4 and 5 with test 7, it can be seen that the first two were characterized by higher values of $G_{\mathrm{n,av}}$ and $G_{\mathrm{bn,av}}$ than the latter. Despite that, their $\Delta t_{\mathrm{h}}$ are higher than that of test 7, showing that $T_{\mathrm{amb}}$ could affect the device performance more than the solar irradiance. In fact, this temperature was much higher in test 7 than in tests 4 and 5 (30.22 °C vs. 21.6 °C and 23.6 °C). However, the influence of a lower solar irradiance is evident in tests 5 and 6 that showed a similar

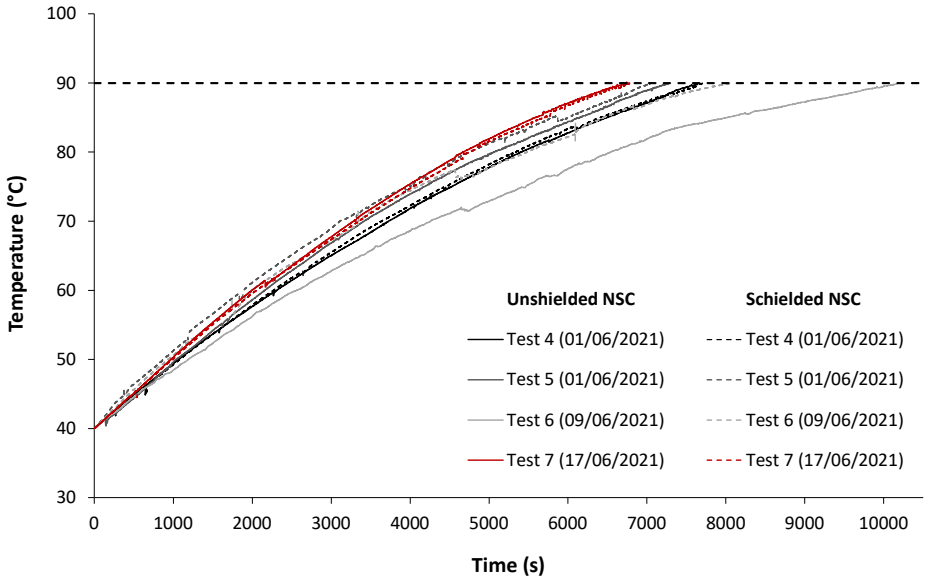


Fig. 9: Water temperature trends.

ambient temperature; in fact, a longer time for water to reach the boiling point was registered in test 6 (average $\Delta t_{\mathrm{h}}$ of 152 min and $G_{\mathrm{n}}$ of 827.54 W/m$^2$) with respect to test 5 (average $\Delta t_{\mathrm{h}}$ of 120 min and $G_{\mathrm{n}}$ of 953.02 W/m$^2$).

To better characterize the devices under investigation, in addition to the average efficiency ($\eta_{\mathrm{av}}$) and the specific and characteristic boiling times ($t_{\mathrm{s}}$ and $t_{\mathrm{c}}$), the following parameters were calculated: the $COR$ parameter and the maximum temperature reachable by the fluid ($T_{\mathrm{fx}}$).

To calculate these parameters, the water temperature range 40–90 °C was divided into sub-intervals of 5 minutes each. For each sub-interval, the averages of the global normal solar irradiance ($G_{\mathrm{n,av}}$), ambient and fluid temperatures ($T_{\mathrm{amb,av}}$ and $T_{\mathrm{f,av}}$), and efficiency ($\eta$) were determined together with the parameter $\chi$. Fig. 10 shows the thermal efficiency $\eta$ plotted against $\chi$ for each identified sub-interval. From the points, it was possible to obtain the regression line of the efficiency curve and its coefficients that correspond to the parameters $F'\eta_0$ (intercept of the line) and $F'U_{\mathrm{l}}/C$ (opposite value of the slope of the line). The $COR$ parameter and $T_{\mathrm{fx}}$ were determined through these two coefficients.

From the parameters calculated for the different tests (Table 5), it can be pointed out that their values for the unshielded device are usually similar to those of the shielded NSC in all the tests. However, it is also possible to note that, while the optical efficiency factor $F'\eta_0$ of the two prototypes is almost constant, the heat loss factor $F'U_l/C$ shows wider variations that depend on the average ambient temperature and wind speed.

### *5.3. Tests with glycerin*

Four outdoor tests were performed by loading each pot with 2 kg of glycerin. Table 6 shows the results obtained for two NSC prototypes in the tests. The parameters reported in this table were calculated in the glycerin temperature range between 40 and 110 °C.

Fig. 11 shows the trends of glycerin temperatures, ambient temperature and global and direct normal solar irradiances recorded on 04/06/2021 (test 9). The average global normal solar irradiances was 963.96 $W/m^2$, while the average ambient temperature was 26.88 °C. The fluid took 199 minutes when tested with the unshielded NSC and 187 minutes when tested with the shielded device to cover the temperature range of 40–110 °C.

Fig. 12 shows the glycerin trends obtained with the unshielded and shielded NSC devices during all the performed tests. From Fig. 12, it is possible to note that, as in the case of the water tests, the curves follow a very similar trend even though the external conditions were different.

However, it is worthwhile noting that the effect of shielding is more evident in the tests with glycerin. In fact, the times required for the fluid to go from 40 to 110 °C were generally longer in the case of the unshielded solar cooker. This is especially evident in tests 8 (03/06/2021) and 10 (22/06/2021): $\Delta t_h$ were 236 and 214 minutes, respectively, for the unshielded NSC and 174 and 175 minutes, respectively, for the shielded NSC.

As for the water tests, to best characterize the two prototypes, the *COR* parameter and $T_{fx}$ were calculated in addition to $\eta_{av}$, $t_s$ and $t_{ch}$. The same procedure described for the water tests was used. The only difference was that the

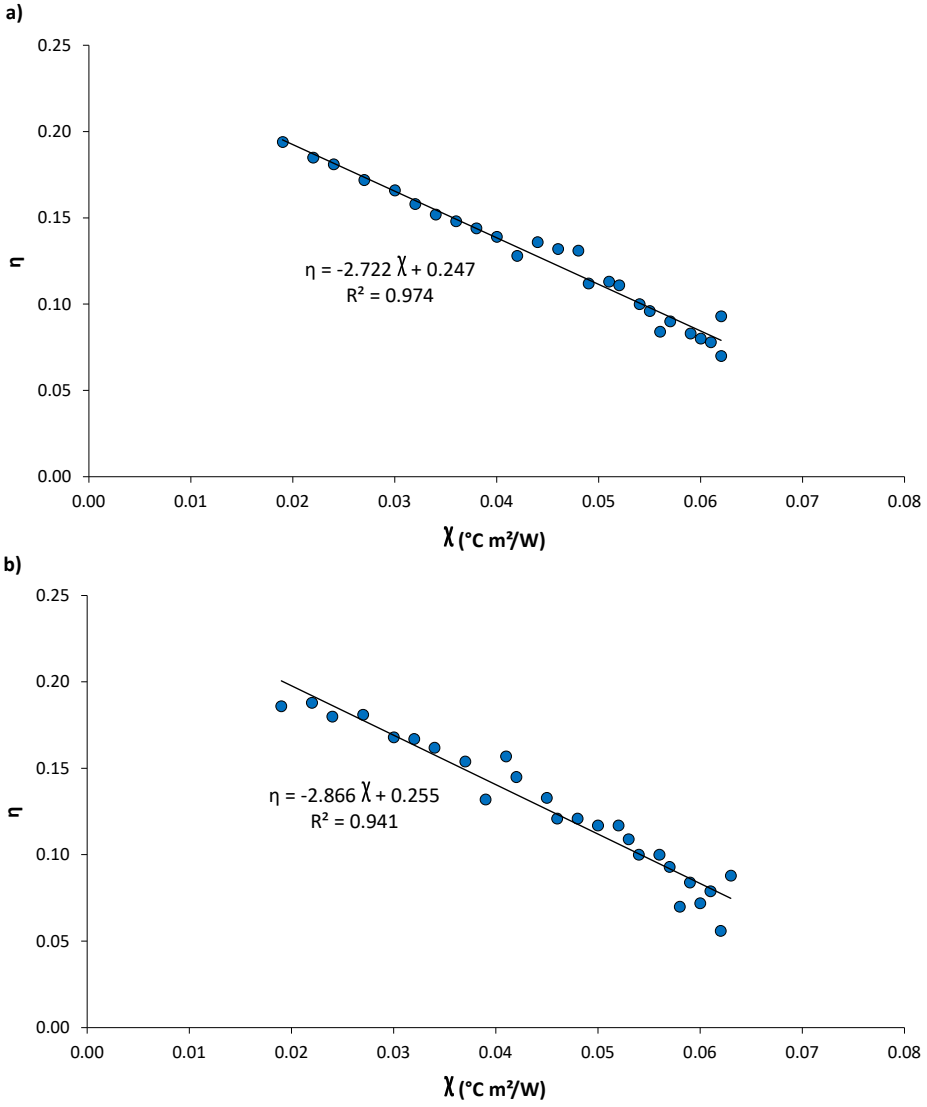


Fig. 10: Efficiency of the cookers tested with water (01/06/2021, test 4): a) unshielded Newton solar cooker and b) shielded Newton solar cooker.

Table 6: Summary of tests with glycerin.

| | Test 8 | | Test 9 | | Test 10 | | Test 11 | |
|---|---|---|---|---|---|---|---|---|
| Date | 03/06/2021 | | 04/06/2021 | | 22/06/2021 | | 29/06/2021 | |
| Type of cooker | Unshielded | Shielded | Unshielded | Shielded | Unshielded | Shielded | Unshielded | Shielded |
| $H_{\mathrm{sun,av}}$ (°) | 60.93 | 60.93 | 60.48 | 60.48 | 63.77 | 63.77 | 61.39 | 61.39 |
| $\theta_{1,\mathrm{av}}$ (°) | 88.69 | 88.69 | 88.53 | 88.53 | 90.98 | 90.98 | 89.19 | 89.19 |
| $\theta_{2,\mathrm{av}}$ (°) | 40.75 | 40.75 | 40.73 | 40.73 | 43.75 | 43.75 | 41.64 | 41.64 |
| $A_{\mathrm{a,av}}$ ($\mathrm{m}^2$) | 0.414 | 0.414 | 0.413 | 0.413 | 0.419 | 0.419 | 0.416 | 0.416 |
| $m_{\mathrm{f}}$ (kg) | 2.0 | 2.0 | 2.0 | 2.0 | 2.0 | 2.0 | 2.0 | 2.0 |
| $T_1$ (°C) | 40 | 40 | 40 | 40 | 40 | 40 | 40 | 40 |
| $T_2$ (°C) | 110 | 110 | 110 | 110 | 110 | 110 | 110 | 110 |
| $G_{\mathrm{n,av}}$ ($\mathrm{W/m}^2$) | 1058.05 | 1048.19 | 962.39 | 965.53 | 934.34 | 934.96 | 910.08 | 910.85 |
| $G_{\mathrm{bn,av}}$ ($\mathrm{W/m}^2$) | 879.44 | 871.25 | 837.81 | 846.06 | 766.25 | 766.75 | 744.91 | 745.54 |
| $T_{\mathrm{amb,av}}$ (°C) | 24.06 | 23.43 | 26.78 | 26.94 | 31.05 | 30.92 | 32.10 | 32.12 |
| $\Delta t_{\mathrm{h}}$ (min) | 236 | 174 | 199 | 187 | 214 | 175 | 140 | 146 |
| $t_{\mathrm{s}}$ ($\mathrm{h\,m}^2/\mathrm{kg}$) | 0.81 | 0.60 | 0.60 | 0.64 | 0.75 | 0.61 | 0.49 | 0.51 |
| $t_{\mathrm{ch}}$ ($\mathrm{h\,m}^2/\mathrm{kg}$) | 0.96 | 0.70 | 0.64 | 0.69 | 0.78 | 0.63 | 0.49 | 0.51 |
| $\eta_{\mathrm{av}}$ | 0.06 | 0.08 | 0.09 | 0.08 | 0.08 | 0.09 | 0.12 | 0.11 |
| $\eta_{\mathrm{u}}$ | 0.08 | 0.10 | 0.11 | 0.10 | 0.09 | 0.10 | 0.13 | 0.13 |
| $F_2$ | 0.12 | 0.17 | 0.19 | 0.18 | 0.15 | 0.19 | 0.24 | 0.24 |
| $F'\eta_0$ | 0.156 | 0.204 | 0.216 | 0.206 | 0.177 | 0.230 | 0.265 | 0.295 |
| $F'U_{\mathrm{l}}/C$ ($\mathrm{W/m}^2\,$°C) | 1.682 | 2.124 | 2.240 | 2.046 | 1.776 | 2.347 | 2.810 | 3.206 |
| $COR$ (°C/($\mathrm{W/m}^2$)) | 0.093 | 0.096 | 0.096 | 0.100 | 0.100 | 0.098 | 0.094 | 0.092 |
| $T_{\mathrm{fx}}$ (°C) | 122.14 | 124.27 | 119.65 | 123.99 | 124.17 | 122.54 | 117.93 | 116.03 |
| $R^2$ | 0.932 | 0.957 | 0.883 | 0.968 | 0.922 | 0.883 | 0.856 | 0.910 |

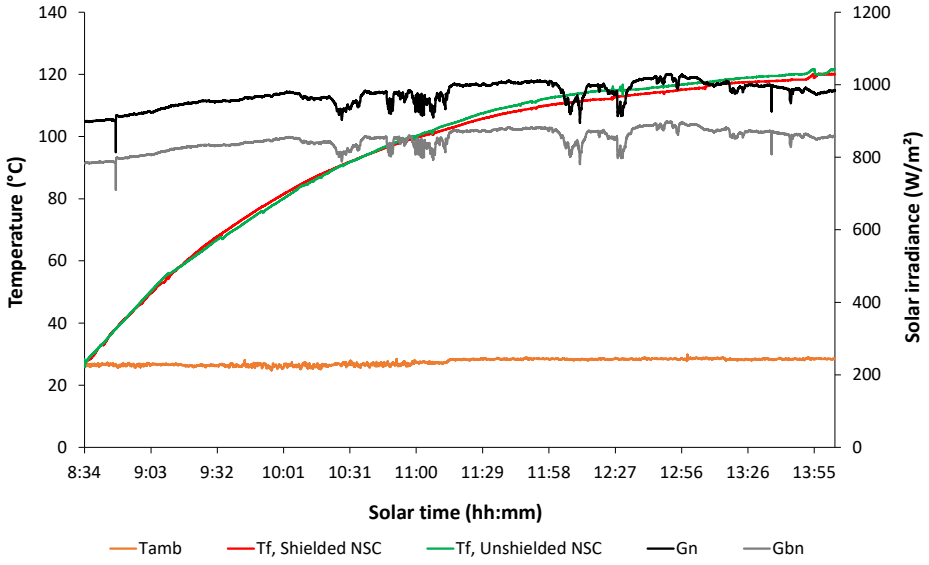


Fig. 11: Test with glycerin (04/06/2021, test 9).

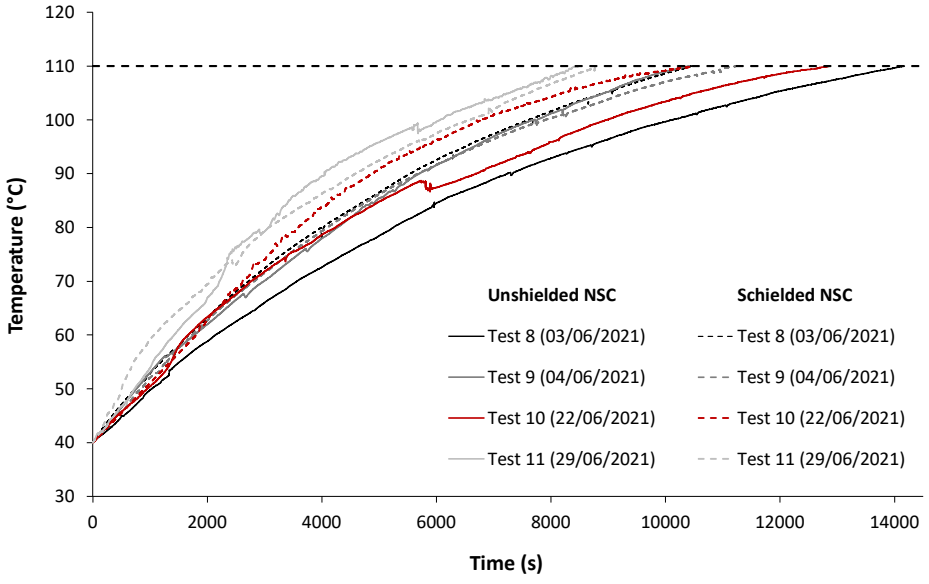


Fig. 12: Glycerin temperature trends.

temperature range from 40 to 110 °C was considered to calculate the parameters.

Fig. 13 shows the efficiency ($\eta$) referring to test 10 (04/06/2021). Also in this case, the values of the calculated parameters are very similar in each test (Table 6). As for the tests with water, the optical efficiency factor ($F'\eta_0$) of the two prototypes is almost constant, while wider variations of the heat loss factor ($F'U_l/C$) are evident.

Finally, from Tables 5 and 6, it can be pointed out that, for the same mass of fluid, the average thermal efficiency ($\eta_{av}$) for the tests with glycerin is lower than that for the tests with water; this outcome can be due to the higher temperatures used to test glycerin.

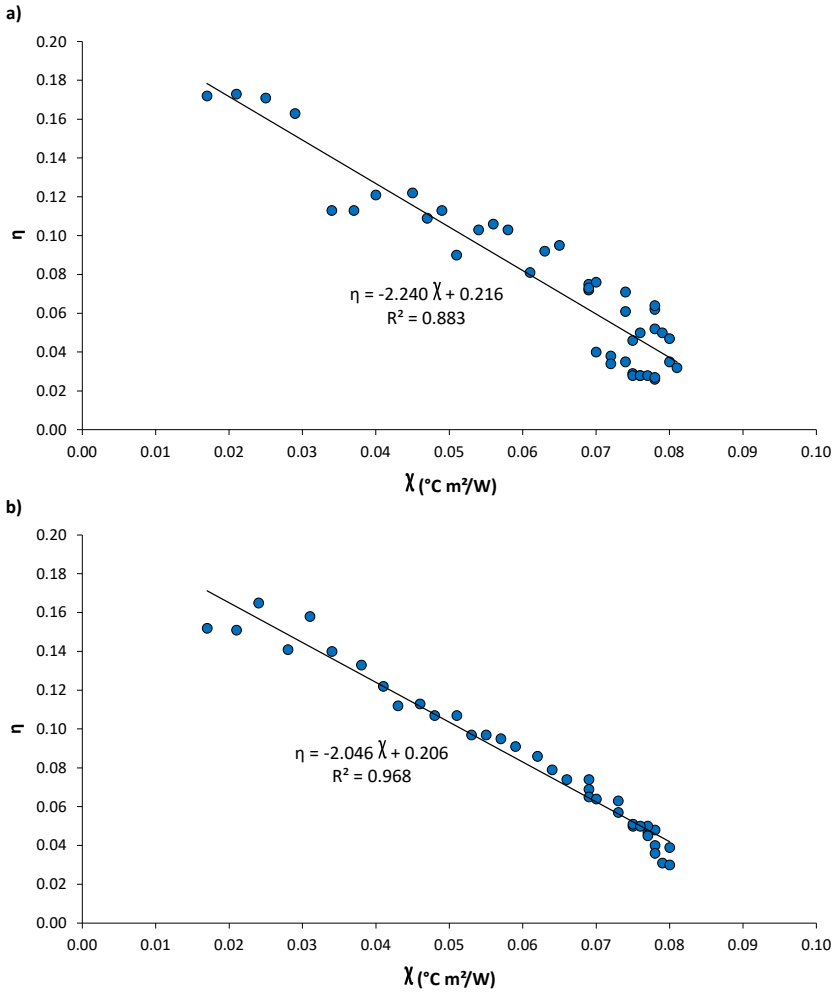


Fig. 13: Efficiency of the cookers tested with glycerin (04/06/2021, test 9): a) unshielded Newton solar cooker and b) shielded Newton solar cooker.

## 6. Conclusions

In this work, a new solar cooker with variable geometry, called Newton solar cooker, was designed, constructed and experimentally tested through an outdoor campaign. The presented device is easy to build, given the few simple steps required in its manufacturing. It is easy to use and transport, given its low weight and the possibility of disassembling the reflective surfaces and folding the reflector supports. In addition, it is mainly made of common and available materials such as wood and glass, making it inexpensive. To track the sun and to maximize the amount of solar radiation concentrated on the cooking chamber, the Newton solar cooker can change the inclination of the reflectors and rotate through wheels.

During the experimental campaign, an unshielded prototype was simultaneously tested with an identical prototype that was shielded from the wind. The two prototypes with tracking reflective surfaces at optimal angles were tested both without load and by loading a pot with water or glycerin. The no-load tests revealed that both prototypes were able to bring the cooker plate to a stagnation temperature of approximately 137 °C. The water tests showed that the shielded Newton solar cooker was capable of boiling 2 kg of water in approximately two hours. This time was slightly longer (on average 133 minutes) in the case of the unshielded device. From the glycerin tests, it was found that, to raise the temperature of 2 kg of glycerin from 40 °C to 110 °C, the shielded Newton solar cooker took 170 minutes on average, while the unshielded device took 197 minutes on average. The use of glycerin showed that the studied cooker can reach medium-high temperatures with good efficiency.

In conclusion, it can be stated that the presented solar cooker is easy to use, cost-effective and non-hazardous thanks to its simplicity and the use of common and recyclable materials. The proposed device is also suited for developing countries where it can be considered as a promising and environmentally friendly alternative to traditional cooking methods.

## Nomenclature

*Latin Symbols*

| | |
|---|---|
| $A$ | Area ($m^2$) |
| $C$ | Concentration ratio |
| $COR$ | Cooker opto-thermal ratio (°C/(W/$m^2$)) |
| $c$ | Specific heat (J/(kg °C)) |
| $F_1$ | First figure of merit (°C/(W/$m^2$)) |
| $F_2$ | Second figure of merit |
| $F'$ | Heat exchange efficiency factor |
| $F'\eta_0$ | Optical efficiency factor |
| $F'U_l$ | Heat loss factor (W/$m^2$ °C) |
| $G$ | Global horizontal solar irradiance (W/$m^2$) |
| $G_{bn}$ | Direct normal solar irradiance (W/$m^2$) |
| $G_n$ | Global normal solar irradiance (W/$m^2$) |
| $H_{sun}$ | Sun elevation (°) |
| $m$ | Mass (kg) |
| $T$ | Temperature (°C) |
| $T_{fx}$ | Maximum achievable fluid temperature (°C) |
| $t$ | Time (min) |

*Greek Symbols*

| | |
|---|---|
| $\eta$ | Efficiency |
| $\eta_0$ | Optical efficiency |
| $\theta$ | Reflector angle (°) |

*Subscripts*

| | |
|---|---|
| a | Absorber, aperture |
| amb | Ambient |
| av | Average |
| ch | Characteristic |
| f | Fluid |
| h | Heating |
| max | Maximum |
| ref | Reference |
| s | Specific, solid |
| u | Utilizable |

*Acronyms*

| | |
|---|---|
| NSC | Newton solar cooker |
| PMMA | Polymethylmethacrylate |

## References

[1] S. Karekezi, W. Kithyoma, Renewable energy strategies for rural Africa: is a PV-led renewable energy strategy the right approach for providing modern energy to the rural poor of sub-Saharan Africa?, Energy Policy 30 (2002) 1071–1086. doi:10.1016/S0301-4215(02)00059-9.

[2] W. Bewket, Household level tree planting and its implications for environmental management in the northwestern highlands of Ethiopia: a case study in the Chemoga watershed, Blue Nile basin, Land Degrad. Dev. 14 (2003) 377–388. doi:10.1002/ldr.559.

[3] G. T. Tucho, S. Nonhebel, Bio-wastes as an alternative household cooking energy source in Ethiopia, Energies 8 (2015) 9565–9583. doi:10.3390/en8099565.

[4] N. Nahar, Performance and testing of a hot box storage solar cooker, Energy Convers. Manage. 44 (2003) 1323–1331. doi:10.1016/S0196-8904(02)00113-9.

[5] M. Aramesh, M. Ghalebani, A. Kasaeian, H. Zamani, G. Lorenzini, O. Mahian, S. Wongwises, A review of recent advances in solar cooking technology, Renew. Energy 140 (2019) 419–435. doi:10.1016/j.renene.2019.03.021.

[6] R. Khatri, R. Goyal, R. K. Sharma, Advances in the developments of solar cooker for sustainable development: a comprehensive review, Renewable and Sustainable Energy Rev. 145 (2021) 111166. doi:10.1016/j.rser.2021.111166.

[7] E. Cuce, P. Cuce, A comprehensive review on solar cookers, Appl. Energy 102 (2013) 1399–1421. doi:10.1016/j.apenergy.2012.09.002.

[8] A. Kundapur, A Treatise on Solar Cookers, first ed., International Alternate Energy Trust, 2018.

[9] A. Khallaf, M. Tawfik, A. El-Sebaii, A. A. Sagade, Mathematical modeling and experimental validation of the thermal performance of a novel design solar cooker, Sol. Energy 207 (2020) 40–50. doi:10.1016/j.solener.2020.06.069.

[10] A. A. Omara, A. A. Abuelnuor, H. A. Mohammed, D. Habibi, O. Younis, Improving solar cooker performance using phase change materi-

als: A comprehensive review, Sol. Energy 207 (2020) 539–563. doi:10.1016/j.solener.2020.07.015.

[11] G. Coccia, A. Aquilanti, S. Tomassetti, P. F. Muciaccia, G. Di Nicola, Experimental analysis of nucleation triggering in a thermal energy storage based on xylitol used in a portable solar box cooker, Energies 14 (2021) 5981. doi:10.3390/en14185981.

[12] U. Arunachala, A. Kundapur, Cost-effective solar cookers: A global review, Sol. Energy 207 (2020) 903–916. doi:10.1016/j.solener.2020.07.026.

[13] Cookit, Solar cooking wiki, Accessed 15 September 2022. URL: https://solarcooking.fandom.com/wiki/CooKit.

[14] SolarFunnelCooker, Solar cooking wiki, Accessed 15 September 2022. URL: https://solarcooking.fandom.com/wiki/Solar_Funnel_Cooker.

[15] HotPot, Solar cooking wiki, Accessed 15 September 2022. URL: https://solarcooking.fandom.com/wiki/HotPot.

[16] Copenhagen, Solar cooking wiki, Accessed 15 September 2022. URL: https://solarcooking.fandom.com/wiki/Copenhagen_Solar_Cooker_Light.

[17] HainesSolarCookers, Solar cooking wiki, Accessed 15 September 2022. URL: https://solarcooking.fandom.com/wiki/Haines_Solar_Cookers.

[18] KyotoBox, Solar cooking wiki, Accessed 17 June 2022. URL: https://solarcooking.fandom.com/wiki/Kyoto_Box.

[19] JoseSol, Solar cooking wiki, Accessed 17 June 2022. URL: https://solarcooking.fandom.com/wiki/Jose_Sol.

[20] H. H. Ozturk, Energy and exergy efficiencies of a solar box-cooker, Int. J. Exergy 1 (2004) 202–214. doi:10.1504/IJEX.2004.005091.

[21] S. Mahavar, N. Sengar, P. Rajawat, M. Verma, P. Dashora, Design development and performance studies of a novel single family solar cooker, Renew. Energy 47 (2012) 67–76. doi:10.1016/j.renene.2012.04.013.

[22] ASAE, Standard 580.1, testing and reporting solar cooker performance, 2013.

[23] S. M. Ebersviller, J. J. Jetter, Evaluation of performance of household solar cookers, Sol. Energy 208 (2020) 166–172. doi:10.1016/j.solener.2020.07.056.

[24] A. A. Sagade, S. Samdarshi, P. Panja, Experimental determination of effective concentration ratio for solar box cookers using thermal tests, Sol. Energy 159 (2018) 984–991. doi:10.1016/j.solener.2017.11.021.

[25] A. A. Sagade, S. Samdarshi, P. S. Panja, Enabling rating of intermediate temperature solar cookers using different working fluids as test loads and its validation through a design change, Sol. Energy 171 (2018) 354–365. doi:10.1016/j.solener.2018.06.088.

[26] A. A. Sagade, S. Samdarshi, P. Lahkar, N. A. Sagade, Experimental determination of the thermal performance of a solar box cooker with a modified cooking pot, Renew. Energy 150 (2020) 1001–1009. doi:10.1016/j.renene.2019.11.114.

[27] A. Weldu, L. Zhao, S. Deng, N. Mulugeta, Y. Zhang, X. Nie, W. Xu, Performance evaluation on solar box cooker with reflector tracking at optimal angle under bahir dar climate, Sol. Energy 180 (2019) 664–677. doi:10.1016/j.solener.2019.01.071.

[28] C. R. Ruivo, A. Carrillo-Andrés, X. Apaolaza-Pagoaga, Experimental determination of the standardised power of a solar funnel cooker for low sun elevations, Renew. Energy 170 (2021) 364–374. doi:10.1016/j.renene.2021.01.146.

[29] X. Apaolaza-Pagoaga, A. Carrillo-Andrés, C. R. Ruivo, Experimental thermal performance evaluation of different configurations of Copenhagen solar

cooker, Renew. Energy 184 (2022) 604–618. doi:10.1016/j.renene.2021.11.105.

[30] C. R. Ruivo, X. Apaolaza-Pagoaga, G. Di Nicola, A. Carrillo-Andrés, On the use of experimental measured data to derive the linear regression usually adopted for determining the performance parameters of a solar cooker, Renew. Energy 181 (2022) 105–115. doi:10.1016/j.renene.2021.09.047.

[31] C. R. Ruivo, X. Apaolaza-Pagoaga, G. Coccia, A. Carrillo-Andrés, Proposal of a non-linear curve for reporting the performance of solar cookers, Renew. Energy (2022). doi:10.1016/j.renene.2022.04.026.

[32] X. Apaolaza-Pagoaga, A. Carrillo-Andrés, C. R. Ruivo, Experimental characterization of the thermal performance of the Haines 2 solar cooker, Energy 257 (2022) 124730. doi:10.1016/j.energy.2022.124730.

[33] G. Coccia, G. Di Nicola, M. Pierantozzi, S. Tomassetti, A. Aquilanti, Design, manufacturing, and test of a high concentration ratio solar box cooker with multiple reflectors, Sol. Energy 155 (2017) 781–792. doi:10.1016/j.solener.2017.07.020.

[34] G. Coccia, A. Aquilanti, S. Tomassetti, A. Ishibashi, G. Di Nicola, Design, manufacture and test of a low-cost solar cooker with high-performance light-concentrating lens, Sol. Energy 224 (2021) 1028–1039. doi:10.1016/j.solener.2021.06.025.

[35] NewtonSolarOven, Solar cooking wiki, Accessed 20 May 2022. URL: `https://solarcooking.fandom.com/wiki/Newton_Solar_Oven`.

[36] NewtonSolarOven2.0, Solar cooking wiki, Accessed 1 June 2022. URL: `https://solarcooking.fandom.com/wiki/Newton_Solar_Oven_2.0`.

[37] MathWorks, Matlab, available online, Accessed 2 June 2022. URL: `https://www.mathworks.com/products/matlab.html`.

[38] MathWorks, Constrained particle swarm optimization, Accessed 2 June 2022. URL: https://www.mathworks.com/matlabcentral/fileexchange/25986-constrained-particle-swarm-optimization.

[39] C. R. Ruivo, X. Apaolaza-Pagoaga, A. Carrillo-Andrés, G. Coccia, Influence of the aperture area on the performance of a solar funnel cooker operating at high sun elevations using glycerine as load, Sustainable Energy Technol. Assess. 53 (2022) 102600. doi:10.1016/j.seta.2022.102600.

[40] S. Kalogirou, Solar Energy Engineering: Processes and Systems, Processes and Systems Series, second edition ed., Elsevier Science, 2013.

[41] S. Mullick, T. Kandpal, A. Saxena, Thermal test procedure for box-type solar cookers, Sol. Energy 39 (1987) 353–360. doi:10.1016/S0038-092X(87)80021-X.

[42] A. Khalifa, M. Taha, M. Akyurt, Solar cookers for outdoors and indoors, Energy 10 (1985) 819–829. doi:10.1016/0360-5442(85)90115-X.

[43] A. El-Sebaii, A. Ibrahim, Experimental testing of a box-type solar cooker using the standard procedure of cooking power, Renew. Energy 30 (2005) 1861–1871. doi:10.1016/j.renene.2005.01.007.

[44] P. Lahkar, R. Bhamu, S. Samdarshi, Enabling inter-cooker thermal performance comparison based on cooker opto-thermal ratio (COR), Appl. Energy 99 (2012) 491–495. doi:10.1016/j.apenergy.2012.05.034.

[45] P. A. Funk, Evaluating the international standard procedure for testing solar cookers and reporting performance, Sol. Energy 68 (2000) 1–7. doi:10.1016/S0038-092X(99)00059-6.

[46] C. R. Ruivo, G. Coccia, G. Di Nicola, A. Carrillo-Andrés, X. Apaolaza-Pagoaga, Standardised power of solar cookers with a linear performance curve following the Hottel-Whillier-Bliss formulation, Renew. Energy (2022). doi:10.1016/j.renene.2022.10.041.

[47] M. Region, Civil protection service, Accessed 2 June 2022. URL: http://84.38.48.145/sol/info.sol?lang=en.

[48] P. Funk, Testing and reporting solar cooker performance, ASAE Standards (2003) 825–826.